Tbx5-dependent pathway regulating diastolic function in congenital heart disease

Yonghong Zhu[a,b], Anthony O. Gramolini[b,c,d], Mark A. Walsh[e], Yu-Qing Zhou[f], Cameron Slorach[e], Mark K. Friedberg[e], Jun K. Takeuchi[a,g], Hui Sun[b], R. Mark Henkelman[f,h], Peter H. Backx[b,d,i,j], Andrew N. Redington[e,k], David H. MacLennan[b,c,l], and Benoit G. Bruneau[a,b,g,l,m]

[a]Programme in Developmental and Stem Cell Biology, [e]Division of Cardiology and Labatt Family Heart Centre, [k]Programme in Physiology and Experimental Medicine, and [f]Mouse Imaging Centre, Hospital for Sick Children, Toronto, ON, Canada M5G 1X8; [c]Banting and Best Department of Medical Research, Charles H. Best Institute, University of Toronto, 112 College Street, Toronto, ON, Canada M5G 1L6; [b]Heart and Stroke/Richard Lewar Centre of Excellence, University of Toronto, Toronto, ON, Canada, M5S 3E2; Departments of [d]Physiology, [m]Molecular and Medical Genetics, [h]Medical Biophysics, and [i]Medicine, University of Toronto, Toronto, ON, Canada M5S 1A8; [j]Division of Cardiology, University Health Network, 190 Elizabeth Street, Toronto, ON, Canada M5G 2C4; and [g]Gladstone Institute of Cardiovascular Disease, Department of Pediatrics, University of California, San Francisco, CA 94158

Contributed by David H. MacLennan, February 22, 2008 (sent for review November 7, 2007)

At the end of every heartbeat, cardiac myocytes must relax to allow filling of the heart. Impaired relaxation is a significant factor in heart failure, but all pathways regulating the cardiac relaxation apparatus are not known. Haploinsufficiency of the T-box transcription factor *Tbx5* in mouse and man causes congenital heart defects (CHDs) as part of Holt–Oram syndrome (HOS). Here, we show that haploinsufficiency of *Tbx5* in mouse results in cell-autonomous defects in ventricular relaxation. *Tbx5* dosage modulates expression of the sarco(endo)plasmic reticulum Ca^{2+}-ATPase isoform 2a encoded by *Atp2a2* and *Tbx5* haploinsufficiency in ventricular myocytes results in impaired Ca^{2+} uptake dynamics and Ca^{2+} transient prolongation. We also demonstrate that Tbx5 can activate the *Atp2a2* promoter. Furthermore, we find that patients with HOS have significant diastolic filling abnormalities. These results reveal a direct genetic pathway that regulates cardiac diastolic function, implying that patients with structural CHDs may have clinically important underlying anomalies in heart function that merit treatment.

calcium | cardiac | transcription | ventricular | SERCA2a

The mammalian heart must beat several thousand times per hour throughout an entire lifetime to circulate blood. An important component of each cardiac cycle is the relaxation of the heart to allow complete filling of the chambers in preparation for the next expulsion of blood. Cardiac relaxation in the ventricles has two components: an active component, during which the muscle actively relaxes after each contraction, followed by a passive component, in which the ventricular chambers distend in response to the influx of blood from the atria. The active component involves highly regulated Ca^{2+} removal from the cytosol to allow dissociation between actin and myosin filaments (1, 2). The major effectors of cardiac relaxation are the sarco(endo)plasmic reticulum Ca^{2+} ATPase isoform 2a (SERCA2a), plasma membrane Ca^{2+} ATPases (PMCAs), and Na^+/Ca^{2+} exchangers (NCXs) (1, 2). Impaired relaxation, or diastolic dysfunction, is an important component of heart failure. Indeed, a significant portion of heart failure patients have normal systolic function, but significantly altered diastolic function (1). Although the roles and importance of the cardiac relaxation machinery have been studied extensively (1–3), and although it is clear that there are alterations in the expression of SERCA2a or NCX1 in cardiomyopathies (1, 4), the regulation of expression of these molecules at the genetic level is not fully understood.

Several transcription factors have been identified as key regulators of cardiac morphogenesis (5, 6), and their importance has been highlighted by the identification of mutations that are causal of inherited congenital heart defects (CHDs) in genes encoding these factors (5, 6). However, defined roles for cardiac transcription factors in regulating pathways critical for normal heart function have been largely elusive, with a few exceptions (7–11).

The T-box transcription factor, Tbx5, is a key regulator of cardiac morphogenesis and gene expression. It is mutated in humans with Holt–Oram syndrome (HOS), a dominant inherited disease characterized by upper limb defects and CHDs (12). The CHDs found in HOS usually arise from atrial or ventricular septation defects or from atrioventricular node conduction system defects. A mouse model of HOS, in which one allele of *Tbx5* was deleted ($Tbx5^{del/+}$ mice), has provided some insight into the etiology of the CHDs caused by Tbx5 haploinsufficiency (7, 13). We observed significant diastolic dysfunction in $Tbx5^{del/+}$ mice (14), suggesting that Tbx5 may be important for regulating components of the cardiac relaxation machinery. However, such relaxation defects might be secondary to volume load alterations because of large atrial septal defects (ASDs) in these mice.

In the present study, we show that *Tbx5* regulates ventricular myocyte relaxation in a cell-autonomous manner by direct modulation of the expression of SERCA2a. Patients with HOS also have diastolic defects that resemble restrictive cardiomyopathy. This defines a Tbx5-dependent pathway for the transcriptional control of diastolic function, with potential implications for the pathogenesis of heart failure and the management of altered heart function in patients with CHDs.

Results

Tbx5 Dosage and Cell-Autonomous Diastolic Dysfunction. $Tbx5^{del/+}$ mice have impaired relaxation as defined by decreased E/A wave ratio and prolonged isovolumic relaxation time (IVRT) measured by Doppler ultrasound (Fig. 1) (14). At the beginning of diastole, early rapid filling of the ventricle results in the E wave, and subsequent atrial contraction results in the A wave. With diastolic abnormalities, both the size and shape of these respective waveforms can change: Early diastolic dysfunction will often result in a prolonged E wave (increased deceleration time) and a decrease in the E/A wave ratio. With progressive diastolic disease and increasing left atrial pressure, this pattern may be reversed (i.e., increasing severity of disease will decrease the E/A ratio). IVRT is prolonged in the early stages of diastolic dysfunction; the myocardium takes longer to relax because of abnormal calcium cycling. In more severe disease states, IVRT

Author contributions: Y.Z. and A.O.G. contributed equally to this work; A.O.G., P.H.B., A.N.R., and B.G.B. designed research; Y.Z., A.O.G., M.A.W., Y.-Q.Z., C.S., M.K.F., J.K.T., and H.S. performed research; R.M.H. contributed new reagents/analytic tools; Y.Z., A.O.G., M.A.W., Y.-Q.Z., J.K.T., H.S., P.H.B., A.N.R., D.H.M., and B.G.B. analyzed data; and A.O.G., D.H.M., and B.G.B. wrote the paper;.

The authors declare no conflict of interest.

[l]To whom correspondence may be addressed. E-mail: david.maclennan@utoronto.ca or bbruneau@gladstone.ucsf.edu.

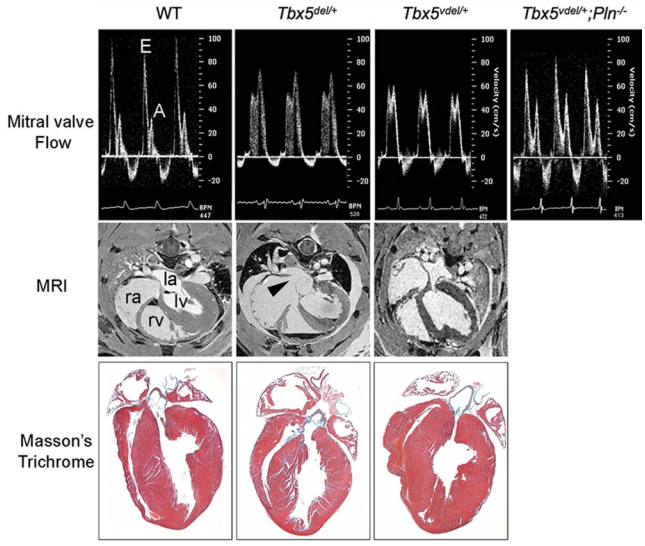

Fig. 1. Diastolic dysfunction in *Tbx5* ventricle-specific haploinsufficient mice. (*Top*) Doppler signal at the MV showing E and A waves. The E wave is decreased, and the A wave is increased in $Tbx5^{del/+}$ and in $Tbx5^{Vdel/+}$ mice. These values are restored to normal in $Tbx5^{Vdel/+}$;$PLN^{-/-}$ mice. (*Middle*) MRI showing ASDs (arrowhead) in $Tbx5^{del/+}$ but not in $Tbx5^{Vdel/+}$ mice. la, left atrium; lv, left ventricle; ra, right atrium; rv, right ventricle. (*Bottom*) Histology of adult hearts stained by Masson's trichrome.

is paradoxically shortened as a result of left atrial hypertension. Smaller left ventricle (LV) end-diastolic diameter (EDD) and end-systolic diameter (ESD) in $Tbx5^{del/+}$ mice also support the finding of impaired diastolic function (14).

Because $Tbx5^{del/+}$ mice have ASDs that alter intracardiac volumes significantly (7, 14), we used a tissue-specific deletion strategy to create haploinsufficiency of *Tbx5* in ventricular myocytes only. Mice bearing loxP-flanked *Tbx5* sequences ($Tbx5^{ldn/ldn}$ mice) (13) and *Nkx2.5-Cre* mice (15), which delete loxP-flanked DNA sequences exclusively in ventricular myocytes from embryonic day 8.5 onward, were bred to generate *Nkx2.5-Cre*;$Tbx5^{ldn/+}$ mice ($Tbx5^{Vdel/+}$ mice). $Tbx5^{Vdel/+}$ mice did not have ASDs or VSDs, nor did they have defects in function of the conduction system (Fig. 1 and Table 1). Doppler ultrasound demonstrated that $Tbx5^{Vdel/+}$ mice also have reduced E/A ratios, albeit less severe than in $Tbx5^{del/+}$ mice, and prolonged IVRT (Fig. 1 and Table 2). M-mode echocardiography also showed reduced LV EDD and ESD (Table 2). Masson's trichrome staining revealed no fibrosis in either $Tbx5^{Vdel/+}$ or $Tbx5^{del/+}$ mice (Fig. 1). Thus, ventricle-restricted haploinsufficiency of *Tbx5* results in diastolic dysfunction.

Tbx5 Modulates SERCA2a Expression. Because *Tbx5* haploinsufficiency results in a cell-autonomous defect in myocyte relaxation, we examined components of the cardiac relaxation machinery.

Table 1. Mouse ECG measurements

Variable	$Tbx5^{+/+}$	$Tbx5^{del/+}$	$Tbx5^{vdel/+}$
Heart rate (min^{-1})	623 ± 39	571 ± 51	660 ± 71
P width	10.8 ± 0.5	17.7 ± 0.4*	10.2 ± 0.3
PQ interval (ms)	31.2 ± 1.9	40.0 ± 0.9*	31.7 ± 1.9
QRS width	12.7 ± 0.91	11.5 ± 1.3	12.4 ± 1.19
Arrhythmias	None	1,2 AVB, sinus pause	None

Telemetry electrocardiogram measurements at 8–10 weeks of age (mean ± SEM); $n = 10–12$; *, $P < 0.05$ vs.WT.

We found a significant decrease in LV protein levels of SERCA2a in $Tbx5^{Vdel/+}$ and $Tbx5^{del/+}$ mice, whereas phospholamban (PLN), Na^+/Ca^{2+} exchanger 1 (NCX1), and ryanodine receptor 2 (RyR2) levels were unaltered (Fig. 2*A*). We observed parallel decreases in mRNA levels of *Tbx5* and *Atp2a2*, which encodes SERCA2a, in LV RNA from $Tbx5^{Vdel/+}$ and $Tbx5^{del/+}$ mice (Fig. 2*B*). SERCA2a functions to pump Ca^{2+} into the SR. Thus, as a functional measure of SERCA2a activity, we measured Ca^{2+} uptake from LV tissue. The rate and amplitude of Ca^{2+} uptake were decreased similarly in $Tbx5^{Vdel/+}$ and $Tbx5^{del/+}$ mice (Fig. 2*C* and Table 3). We also measured Ca^{2+} transients in isolated LV myocytes, detecting a normal amplitude, but a decreased rate of decay of the Ca^{2+} transients in myocytes from $Tbx5^{del/+}$ and $Tbx5^{Vdel/+}$ mice (Fig. 2*D* and data not shown). Overall, these results are consistent with impaired SR Ca^{2+} cycling in LV cardiac myocytes because of decreased SERCA2 levels in $Tbx5^{Vdel/+}$ and $Tbx5^{del/+}$ mice.

If the defects in diastolic function are truly specific to altered SERCA2a, they should be reversible upon deletion of *PLN*, a negative regulator of SERCA2a function (2), which would lead to a specific increase in the affinity of SERCA2a for Ca^{2+}. Indeed, $Tbx5^{Vdel/+}$;$PLN^{-/-}$ mice had normal diastolic function (Fig. 1 and Table 1) and increased rates of Ca^{2+} uptake that were intermediate between wild-type mice and those seen in $PLN^{-/-}$ hearts (Fig. 2*C* and Table 3). Interestingly, we also observed increased SERCA2a protein levels in $Tbx5^{vdel/+}$;$PLN^{-/-}$ hearts, suggesting that a feedback mechanism involving Ca^{2+} also might regulate SERCA2a transcription. It is not clear how this feedback mechanism might function, but recent data have demonstrated that intracellular signaling pathways, including Ca^{2+}, can potentiate the activity of certain transcription factors (16–18), and Ca^{2+} channels themselves can act as transcription factors in a Ca^{2+}-dependent manner (19). Thus, the transcriptional regulation of *Atp2a2* by Tbx5 may not reach its full potential under the conditions of abnormal Ca^{2+} regulation imposed by suboptimal levels of SERCA2a. When Ca^{2+} regulation is restored in $Tbx5^{vdel/+}$;$PLN^{-/-}$ hearts by a sharpening of the curve of Ca^{2+} decay, the full potential of *Tbx5* as a transcription factor may then be realized. Alternatively, altered Ca^{2+} kinetics might affect pathways parallel to *Tbx5* that also are important for the regulation of SERCA2a expression. Regardless of this potential additional mechanism, the fact that SERCA2a protein and mRNA are decreased specifically in parallel with *Tbx5* dosage, and that this is rescued by ablation of PLN, supports the view that the defects in diastolic function caused by a decreased dosage of *Tbx5* are due to a specific effect on SR Ca^{2+} cycling via the down-regulation of SERCA2a levels, leading to a decrease in total SERCA2a activity.

We isolated genomic sequences upstream of mouse *Atp2a2*, including 4 kb of upstream sequences and the endogenous promoter, and fused them to the *luciferase* reporter gene. Cotransfection of the *Atp2a2-luciferase* reporter constructs with a Tbx5 expression construct showed that sequences up to 4 kb upstream of the *Atp2a2* transcriptional start site conferred activation of the reporter gene in response to exogenously added Tbx5 (Fig. 2*E*). Thus, *Atp2a2* is likely to be a direct, dosage-sensitive target of Tbx5 in cardiac myocytes.

Diastolic Defects in HOS Patients. Our findings suggest that haploinsufficiency of *TBX5* in humans also should result in diastolic filling abnormalities. We analyzed a cohort of HOS patients and age-matched controls by Doppler ultrasound. Of 13 patients suitable for enrollment in the study, 8 participated. HOS was diagnosed clinically in all patients (Table 4). One had a *TBX5* mutation, whereas the others did not have genetic testing. Both pulsed Doppler of the mitral inflow and LV tissue Doppler showed significant differences between the HOS patients and the control group (Fig. 3 and Table 5). In patients with HOS, the

Table 2. Systolic and diastolic function in mice

Variable	*Tbx5*$^{+/+}$	*Tbx5*$^{Vdel/+}$	*Tbx5*$^{Vdel/+}$;*PLN*$^{-/-}$	*PLN*$^{-/-}$
Body weight, g	29.1 ± 1.0	27.8 ± 1.1	26.1 ± 4.4	27.9 ± 6.5
Heart rate, min^{-1}	403 ± 10	395 ± 9	422 ± 39	440 ± 32
LV end-diastole				
AW, mm	0.85 ± 0.03	0.92 ± 0.02	0.99 ± 0.06	0.82 ± 0.03
EDD, mm	4.22 ± 0.08	3.79 ± 0.09*‡	4.02 ± 0.10	4.32 ± 0.14*
PW, mm	0.72 ± 0.02	0.71 ± 0.03	0.80 ± 0.07	0.71 ± 0.03
LV end-systole				
AW, mm	1.20 ± 0.05	1.28 ± 0.04	1.26 ± 0.08	1.08 ± 0.08
ESD, mm	2.89 ± 0.11	2.71 ± 0.13	2.82 ± 0.19	2.94 ± 0.09
PW, mm	0.98 ± 0.04	0.97 ± 0.06	1.15 ± 0.08	0.99 ± 0.03
LV FS, %	35.1 ± 2.5	32.1 ± 0.13	32.6 ± 1.2	36.7 ± 0.9
E wave	816 ± 29	670 ± 54*†‡	820 ± 31	854 ± 8
A wave	418 ± 23	527 ± 21*	479 ± 22	458 ± 10
E/A	2.05 ± 0.07	1.27 ± 0.08*†‡	1.71 ± 0.07*	1.87 ± 0.05
IVRT	15.7 ± 0.57	19.1 ± 0.39*†‡	14.9 ± 0.45	13.8 ± 0.33
DT	69.7 ± 3.4	47.7 ± 1.0*†‡	72.2 ± 3.3	75.3 ± 1.1
IVRT/DT	0.22 ± 0.01	0.40 ± 0.01*†‡	0.20 ± 0.01	0.18 ± 0.01

Cardiac M mode and Doppler ultrasound measurements at 8–10 weeks of age (mean ± SEM); $n = 10–12$; *, $P <$ 0.05 vs. WT; †, $P < 0.05$ vs. *Tbx5*$^{Vdel/+}$;*PLN*$^{-/-}$; ‡, $P < 0.05$ vs *PLN*$^{-/-}$.

early diastolic flow (E wave) was increased ($P = 0.003$), the late diastolic flow (A wave) was decreased ($P = 0.026$), with the early/late ratio increased ($P = 0.001$). Although IVRT was prolonged in some patients, the trend did not achieve overall statistical significance ($P = 0.13$). Tissue Doppler velocities were decreased in all areas, but were most notable in the interven-

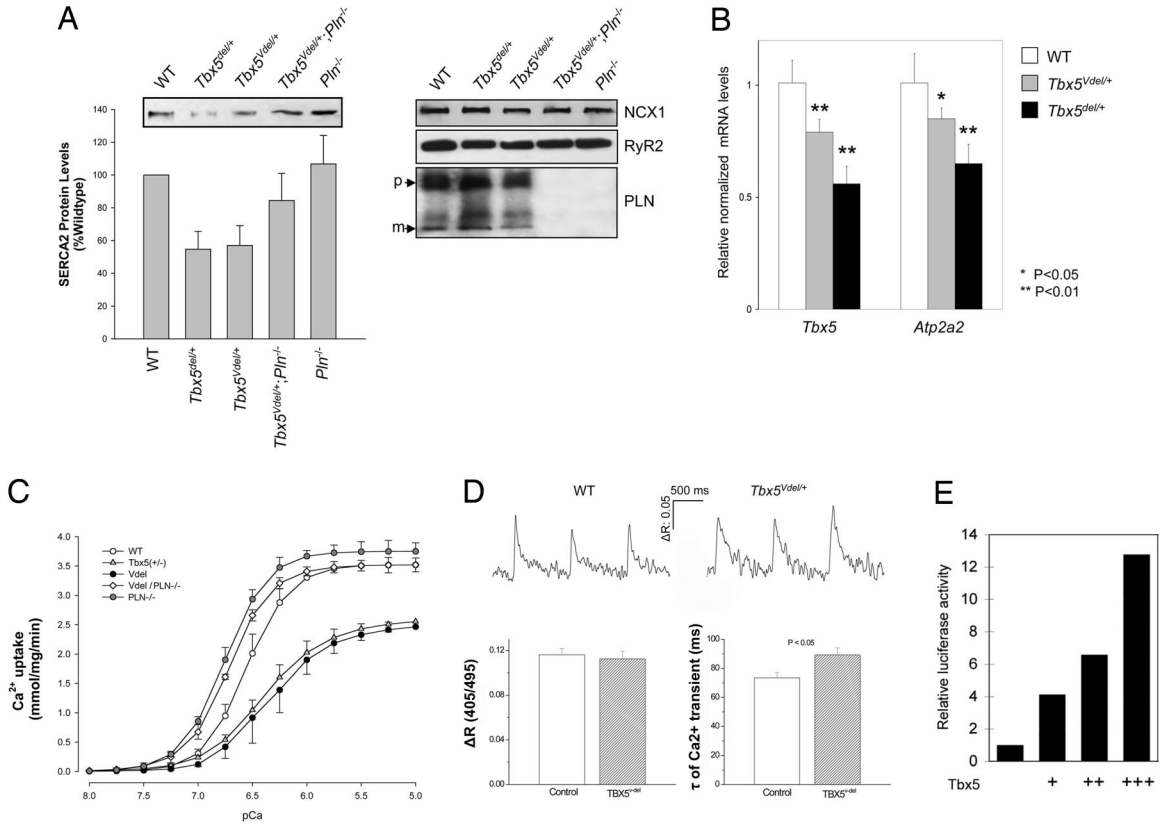

Fig. 2. Tbx5 modulates SERCA2 expression. (*A*) Western blots showing decreased levels of SERCA2 protein in *Tbx5*$^{del/+}$ and *Tbx5*$^{Vdel/+}$ ventricular extracts. Normal levels of Ncx1, RyR2, and PLN were found in all genotypes. (*B*) Quantitative RT-PCR demonstrating decreased *Tbx5* and *Atp2a2* mRNA levels in *Tbx5*$^{del/+}$ and *Tbx5*$^{Vdel/+}$ ventricular extracts ($n = 6$ for each genotype; means ± SEMs are shown). *, $P < 0.05$; **, $P < 0.01$. (*C*) Ca^{2+} uptake in ventricular tissues demonstrating impaired Ca^{2+} uptake in *Tbx5*$^{del/+}$ and *Tbx5*$^{Vdel/+}$ mice and restoration to WT levels in *Tbx5*$^{Vdel/+}$;*PLN*$^{-/-}$ mice. (*D*) Intracellular Ca^{2+} transients. (*Upper*) Representative Ca^{2+} transient recordings obtained from control and *Tbx5*$^{Vdel/+}$ cardiomyocytes under field stimulation at 1 Hz (35.5 ± 0.5°C) and loaded with indo 1-AM. ΔR stands for $\Delta R_{405/495}$, the ratio of the intensity of fluorescence emitted at 405 nm to that at 495 nm, which is used as an index of intracellular Ca^{2+} concentrations in this study. (*Lower*) Mean data of Ca^{2+}-transient amplitude ($\Delta R_{405/495}$) and time constant (τ) of Ca^{2+} transient decay (in milliseconds) obtained from myocytes isolated from control ($n = 41$ cells) and *Tbx5*$^{Vdel/+}$ ($n = 43$ cells) mice. (*E*) Luciferase reporter assay shows dosage-dependent activation of *Atp2a2-luciferase*. Expression vectors: +, 100 ng; ++, 250 ng; +++, 500 ng.

Table 3. Ca^{2+} uptake measurements

	n	K_{Ca} ($_pCa$ units)	Δ K_{Ca}	Vmax, nmol/mg/min
WT	5	6.54 ± 0.07	—	3.36 ± 0.23
Tbx5$^{del/+}$	5	6.32 ± 0.09*†‡	−0.22	2.56 ± 0.18*†‡
Tbx5$^{Vdel/+}$	4	6.22 ± 0.14*†‡	−0.19	2.46 ± 0.04*†‡
Tbx5$^{Vdel/+;PLN-/-}$	4	6.73 ± 0.06	0.19	3.52 ± 0.51
PLN$^{-/-}$	8	6.80 ± 0.06	0.26	3.75 ± 0.33

*, $P < 0.05$ vs. WT; †, $P < 0.05$ vs. *Tbx5*$^{Vdel/+}$;*PLN*$^{-/-}$; ‡, $P < 0.05$ vs. *PLN*$^{-/-}$.

tricular septum (IVS) ($P = 0.005$). The E/E′ ratio was increased for the mitral valve (MV) ($P = 0.03$) and more markedly at the IVS ($P = 0.0001$), indicating a restrictive pattern of filling.

The severity and type of diastolic filling abnormalities was quite variable in our human subjects. To illustrate individual cases, we compared echocardiogram data to published normal values (Table 6) (20). Patient 1 was 12 years old and had small intracardiac lesions that closed spontaneously. The pattern of diastolic filling abnormalities seen was similar to that of the mouse model; deceleration time was prolonged (197 ms; >2 SD from mean), but IVRT was within normal limits (Table 6). Tissue Doppler measurements were marginally low. More notably, however, both of the corresponding E/E′ ratios showed a marked increase. There also was the prominent reversal of flow in the pulmonary veins during atrial systole, another marker of diastolic filling abnormality. This pattern suggests early relaxation abnormalities (prolonged deceleration time), which may be progressing to a more restrictive pattern of diastolic filling (elevated E/E′ ratio). Patient 4 had a structurally normal heart, yet his echocardiogram findings are consistent with a restrictive cardiomyopathy.

Discussion

In the present work, we showed that *Tbx5* regulates cardiac myocyte relaxation properties by direct regulation of SERCA2 protein levels. This establishes a pathway in the regulation of cardiac diastolic function, with potential implications for the management of CHD patients.

Our identification of *Tbx5* as a dosage-sensitive regulator of *Atp2a2* gene expression provides a key entry point in uncovering pathways that modulate cardiac relaxation and SR Ca^{2+} cycling from a transcriptional perspective. To date, the transcriptional pathways that regulate the molecular components of the cardiac myocyte relaxation machinery have remained elusive. There have been suggestions that Sp1 or related factors are involved in the decreased expression of *Atp2a2* in cardiac hypertrophy (21) and that ATF6 increases *Atp2a2* mRNA under stress conditions (22). However, no endogenous transcription factor has been shown to be critical for *in vivo* regulation of *Atp2a2* or other components of the cardiac myocyte relaxation machinery.

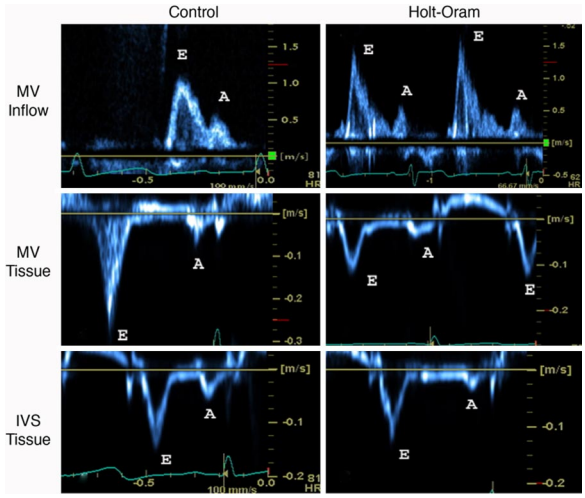

Fig. 3. Doppler ultrasound shows diastolic dysfunction in patients with HOS. Measurements are made from the four-chamber view; the pulsed Doppler sample is placed on the MV orifice, the MV annulus, and the IVS. The MV inflow pattern (*Top*) and tissue Doppler patterns for the MV (*Middle*) and IVS (*Bottom*) are shown in a patient with HOS (*Right*) compared with an age-matched control (*Left*). All measurements are in ms. The MV inflow pattern shows a larger E wave in the patient with HOS; tissue velocities for the MV and IVS tissue also are lower. Compared with the age-matched control, this indicates a more restrictive pattern of filling.

Significantly, our results suggest that the function of Tbx5 is not necessarily restricted to the embryo. The importance of the persistent expression of key developmental transcription factors into adulthood is becoming clearer. Recently, the requirement for *Nkx2-5* in postnatal cardiac growth and function has been demonstrated (9). Mice with a ventricular myocyte-restricted deletion of *Nkx2-5* have a range of defects that includes conduction system disease and cardiomyopathy. Similarly, mice with ablation of the *Homeodomain-only protein* (*Hop*) gene have postnatal ECG anomalies that reflect the predominant postnatal expression of Hop in the conduction system (11). Finally, postnatal deletion of the zinc-finger transcription factor, Gata4, has shown that it plays a role in regulating contractile and diastolic function, and it also is required for adaptative hypertrophy after pressure overload (23, 24). In these cases, functional deficiencies were accompanied by increased fibrosis and apoptosis, suggesting that they were secondary events. In the case of Tbx5, our results uncovered a cell-autonomous, dosage-specific postnatal role, which is distinct from the complete loss of function that the above-mentioned studies have described. Thus, Tbx5 may have a specific and prominent role in regulating the postnatal diastolic function of the heart.

Table 4. Clinical characteristics of the HOS patients studied

No.	Age	*TBX5*	Cardiac	Limb malformations	VSD	ASD
1	12	N/A	VSD and ASD closed	Bilateral radial abnormalities	Yes	No
2	6	N/A	ASD closed	Bilateral radial and thumb abnormalities	No	No
3	20	N/A	Small VSD now closed	Yes; no specific details available	No	No
4	5	Deletion	Tiny VSD	Small hands with three digits, rudimentary humeri bilaterally	Yes	No
5	22	N/A	ASD with surgical closure	Bilateral dysplastic thumbs	No	No
6	22	N/A	PFO	Bilateral radial deformity	No	Yes
7	18	N/A	Small PFO	Bilateral thumb hypoplasia	No	No
8	18	N/A	Structurally normal heart	Bilateral radial abnormalities	No	No

VSD, ventricular septal defect; ASD, atrial septal defect; PFO, patent foramen ovale.

Table 5. Systolic and diastolic function in humans

	HOS ($n = 8$)	Controls ($n = 8$)	P
Age, years	11.25 ± 5.1	15.2 ± 6.8	0.14
Body weight, kg	53.8 ± 26.1	44.2 ± 18.8	0.31
Heart rate, beats/min	96 ± 17	99 ± 11	0.8
Shortening fraction, %	35 ± 4.1	34.7 ± 3.2	0.89
Mitral valve inflow			
E wave, cm/s	123 ± 22	159 ± 21	0.03
A wave, cm/s	45 ± 8	52 ± 8	0.026
E/A ratio	2.8 ± 0.7	2 ± 0.3	0.003
Deceleration time	170 ± 18	159 ± 21	0.24
IVRT	69 ± 10	62 ± 14	0.13
Tissue Doppler			
MV-E′, cm/s	18.1 ± 4.3	21.2 ± 3.2	0.049
MV-A′, cm/s	5.5 ± 2.3	7.1 ± 1.1	0.06
MV-E/E′, cm/s	7.1 ± 2.7	4.9 ± 0.75	0.03
IVS-E′, cm/s	11 ± 1.5	16 ± 2.9	0.005
IVS-A′, cm/s	4.8 ± 1.9	6.4 ± 1.2	0.05
IVS-E/E′, cm/s	11.3 ± 3	4.9 ± 0.77	0.0001

E wave, early mitral inflow; A wave, late mitral inflow; IVRT, isovolumic relaxation time; MV-E′ and MV-A′, mitral annulus early (E′) and late (A′) myocardial velocities; IVS-E′ and IVS-A′, interventricular septum early (E′) and late (A′) myocardial velocities; E/E′ ratio, inflow velocity divided by the tissue Doppler velocity.

Our results show that HOS in humans also is associated with altered diastolic function. The prolonged isovolumic relaxation time is compatible with early diastolic impaired relaxation, similar to *Tbx5* haploinsufficient mice, although the difference failed to reach overall significance. The remaining indices suggest abnormal chamber compliance and myocardial stiffness. Most notably, the E/E′ (the best available index of myocardial stiffness) (25) was elevated in our patients. Overall, some discordance was seen between the diastolic phenotype observed in our mouse model and humans. This result is to be expected given the progressive nature of diastolic dysfunction in clinical syndromes and differences in physiological adaptation in mice and humans. Furthermore, the temporal progression from abnormal relaxation to pseudonormalization to an overtly restrictive late diastolic pattern of dysfunction is well described in many disease states (26). Although there is some evidence of a persisting relaxation abnormality, our data suggest that, in the long term, diastolic disease in HOS may evolve to a predominantly late-diastolic abnormality consistent with increased LV myocardial stiffness. Nevertheless, our patients were clinically asymptomatic, which is not surprising given the magnitude of the diastolic filling abnormalities in this relatively young population. Individuals (Table 6) fulfilled accepted criteria for diastolic filling abnormalities, highlighting the variable expressivity of *TBX5* mutations in human disease.

Table 6. Echocardiogram findings of individual patients

	Patient 1	Patient 4	95% C.I.
Mitral valve inflow			
E wave, cm/s	138*	150*	62.5–127
A wave, cm/s	48	55	22–77
E/A ratio	2.9*	2.7*	1.4–2.6
Deceleration time	197*	183	119–195
IVRT	60	83	47–87
Tissue Doppler			
MV-E′	16.6	12.6	12.8–26.4
MV-A′	8.2	3.7	2.8–10
MV-E/E′	8.3*	11.9*	3.6–6.2
IVS-E′	8.4*	13.5	9.3–17.9
IVS-A′	4	3.7	1.5–10.7
IVS-E/E′	16.4*	11.1*	3.8–9.4
Pulmonary vein Doppler			
A-wave reversal	40*	None	11–31

E wave, early mitral inflow; A wave, late mitral inflow; IVRT, isovolumic relaxation time; MV-E′ and MV-A′, mitral annulus early (E′) and late (A′) myocardial velocities; IVS-E′ and IVS-A′, interventricular septum early (E′) and late (A′) myocardial velocities; E/E′ ratio, inflow velocity divided by the tissue Doppler velocity; A-wave reversal, peak velocity of retrograde blood flow in the pulmonary vein during atrial systole. *, $P < 0.05$ vs. healthy patient data.

The identification of a Tbx5-dependent pathway in the regulation of postnatal diastolic function has several clinical implications. First, it provides an entry point to understand the regulation of the molecular components critical for normal diastolic function. Second, diastolic dysfunction in *Tbx5* haploinsufficient mice occurs without any other defect in heart structure or function. Therefore, our understanding of a specific component of heart failure will be greatly enhanced by elucidating the role of *Tbx5* in this specific component of heart failure. Third, our finding may have direct implications for the management of patients with corrected CHDs. Congenital defects are well known to have severe sequelae, and patients may progress to heart failure in adulthood even after successful childhood closure of a septal defect (27–29). Our results suggest that this may be caused, in part, by impaired diastolic function from abnormal regulation of SERCA2 or other components that regulate myocyte relaxation. In support of this notion, ultrasound measurement of heart chamber volumes *in utero* has shown a significantly reduced EDD in fetuses with CHDs, compared with normal controls (30). Furthermore, a recent study has shown that patients with ASDs do not recover normal diastolic function after ASD closure, indicating the possibility of an underlying primary defect (31). Moreover, in patients with Marfan syndrome, primary LV dysfunction has been reported, suggesting that underlying, clinically significant defects in heart function, unrelated to structural anomalies, may be widespread (32). Finally, ventricular deletion of *Nkx2-5* in the mouse uncovered a pathway for cardiac growth that implied continued requirement for *Nkx2-5* in ventricular myocytes. This finding was extended to patients with *NKX2-5* mutations, which in some cases led to heart failure (9).

Because we have found defects in diastolic function in humans with HOS that are similar to those in the mice, it is very likely that we have uncovered a pathway that has direct relevance to CHD patients. An ascertainment of the global relevance of the current findings to a clinical setting will require evaluation of a large cohort of patients with congenital heart defects of defined and varied genetic etiology.

Materials and Methods

Mouse Lines and Characterization. *Tbx5*$^{ldn/ldn}$, Nkx2.5Cre mice, and *PLN*$^{+/-}$ were generated as described (13, 15, 33). MRI, ultrasound, and histology were performed as described (13, 14).

Antibodies and Immunoblots. mAb 1D11 was kindly provided by R. Johnson (Merck Laboratories, West Point, PA). mAB IID8F6 against SERCA2 was a gift from K. Campbell (University of Iowa, Iowa City, IA). mAb NXC1 (SWANT) and mAb ryanodine receptor 2 (Affinity Bioreagents) were obtained commercially. Mouse ventricles were isolated, washed in PBS, and homogenized in 250 mM sucrose, 50 mM Tris·HCl (pH 7.4), 1 mM PMSF, and 20 μg/ml aprotinin. Lysates were isolated after a 15-min centrifugation at 8,000 × *g*, and the supernatant was collected and used. Immunoblots were performed as described (34). Membrane signals were quantified by using a BioRad Fluor-S Multiimager documentation system.

Ca^{2+} Transport. ATP and oxalate-dependent Ca^{2+} uptake activities in whole-heart homogenates were measured by using a Millipore filtration method (35,

36). The Ca^{2+} concentration required for half-maximal velocity for Ca^{2+} uptake (EC_{50}) was determined by nonlinear curve fitting.

Human Echocardiographic Studies. After approval from the Research and Ethics Board at the Hospital for Sick Children, we searched both cardiac and genetic databases for patients with HOS. Exclusion criteria were a pacemaker, significant structural cardiac abnormalities, those with previous surgical intervention other than an atrial septal defect closure, and non-HOS clinical features (37). Eligible patients were contacted to enroll in the study, which involved an echocardiogram to evaluate diastolic function. Age-matched controls were selected from a previous study, all of whom had normal parameters of diastolic function. All studies were carried out with the VIVID 7 Vantage System (General Electric) by the same operator. Mitral valve inflow patterns were recorded with pulsed Doppler; tissue Doppler velocities were measured from the MV annulus and the IVS, all in the four-chamber view. Early mitral inflow (E wave), late mitral inflow (A wave), isovolumic relaxation time, E wave deceleration time, and early (E′) and late (A′) myocardial velocities (mitral annulus and IVS) were recorded. In addition, we calculated the E/E′ ratio (i.e., MV inflow velocity divided by the mitral annulus tissue Doppler velocity), which is elevated in conditions where there is restrictive LV filling (25).

Statistics. Data are presented as mean ± SEM. In all cases, results are from a minimum of three separate experiments. Comparisons were by Student's *t* test or ANOVA, followed by an appropriate post hoc test. For the human studies, Wilcoxon's rank test for nonnormal data were used to compare the two groups. All statistical analyses were performed with SPSS version 12.0. P values < 0.05 were considered significant.

ACKNOWLEDGMENTS. We thank Dr. Eric N. Olson (University of Texas Southwestern Medical Center) for generously providing the *Nkx2.5*::*Cre* transgenic mice and Dr. Evangelia Kranias (University of Cincinnati, Cincinnati, OH) for generously providing the $Pln^{+/-}$ mice. This work was supported by Heart and Stroke Foundation of Ontario (HSFO) Grant N-5449 (to B.G.B.), March of Dimes Birth Defects Foundation Grant 1-FY05-1261 (to B.G.B.), HSFO Grant T-5042 (to D.H.M.), Canadian Institutes of Health Research Grant MT-12545 (to D.H.M.), a Canada Research Chair in Developmental Cardiology (B.G.B.), a Canada Research Chair in Imaging (R.M.H.), and an HSFO Fellowship and New Investigator award (to A.O.G.).

1. Kass DA, Bronzwaer JG, Paulus WJ (2004) What mechanisms underlie diastolic dysfunction in heart failure? *Circ Res* 94:1533–1542.
2. MacLennan DH, Kranias EG (2003) Phospholamban: A crucial regulator of cardiac contractility. *Nat Rev Mol Cell Biol* 4:566–577.
3. Maclennan DH (2004) Interactions of the calcium ATPase with phospholamban and sarcolipin: Structure, physiology and pathophysiology. *J Muscle Res Cell Motil* 25:600–601.
4. Dillmann WH (1996) Regulation of expression of cardiac sarcoplasmic reticulum proteins under pathophysiological conditions. *Mol Cell Biochem* 157:125–128.
5. Srivastava D (2006) Making or breaking the heart: From lineage determination to morphogenesis. *Cell* 126:1037–1048.
6. Bruneau BG (2008) The developmental genetics of congenital heart disease. *Nature* 451:943–948.
7. Bruneau BG, *et al.* (2001) A murine model of Holt-Oram syndrome defines roles of the T-box transcription factor Tbx5 in cardiogenesis and disease. *Cell* 106:709–721.
8. Naya FJ, *et al*. (2002) Mitochondrial deficiency and cardiac sudden death in mice lacking the MEF2A transcription factor. *Nat Med* 8:1303–1309.
9. Pashmforoush M, *et al.* (2004) Nkx2-5 pathways and congenital heart disease: Loss of ventricular myocyte lineage specification leads to progressive cardiomyopathy and complete heart block. *Cell* 117:373–386.
10. Costantini D, *et al.* (2005) The homeodomain transcription factor Irx5 establishes the mouse cardiac ventricular repolarization gradient. *Cell* 123:347–358.
11. Ismat FA, *et al*. (2005) Homeobox protein Hop functions in the adult cardiac conduction system. *Circ Res* 96:898–903.
12. Mori AD, Bruneau BG TBX5 mutations and congenital heart disease: Holt-Oram syndrome revealed. *Curr Opin Cardiol* 19:211–215.
13. Mori AD, *et al.* (2006) Tbx5-dependent rheostatic control of cardiac gene expression and morphogenesis. *Dev Biol* 297:566–586.
14. Zhou YQ, *et al*. (2005) Abnormal cardiac inflow patterns during postnatal development in a mouse model of Holt-Oram syndrome. *Am J Physiol* 289:H992–H1001.
15. McFadden DG, *et al*. (2004) The Hand1 and Hand2 transcription factors regulate expansion of the embryonic cardiac ventricles in a gene dosage-dependent manner. *Development* 132:189–201.
16. Wu X, *et al*. (2006) Local InsP3-dependent perinuclear Ca^{2+} signaling in cardiac myocyte excitation–transcription coupling. *J Clin Invest* 116:675–682.
17. Backs J, Song K, Bezprozvannaya S, Chang S, Olson EN (2006) CaM kinase II selectively signals to histone deacetylase 4 during cardiomyocyte hypertrophy. *J Clin Invest* 116:1853–1864.
18. Song K, *et al*. (2006) The transcriptional coactivator CAMTA2 stimulates cardiac growth by opposing class II histone deacetylases. *Cell* 125:453–466.
19. Gomez-Ospina N, Tsuruta F, Barreto-Chang O, Hu L, Dolmetsch R (2006) The C terminus of the L-type voltage-gated calcium channel Ca(V)1.2 encodes a transcription factor. *Cell* 127:591–606.
20. Eidem BW, *et al*. (2004) Impact of cardiac growth on Doppler tissue imaging velocities: A study in healthy children. *J Am Soc Echocardiogr* 17:212–221.
21. Takizawa T, *et al*. (2003) Transcription factor Sp1 regulates SERCA2 gene expression in pressure-overloaded hearts: A study using *in vivo* direct gene transfer into living myocardium. *J Mol Cell Cardiol* 35:777–783.
22. Thuerauf DJ, *et al*. (2001) Sarco/endoplasmic reticulum calcium ATPase-2 expression is regulated by ATF6 during the endoplasmic reticulum stress response: Intracellular signaling of calcium stress in a cardiac myocyte model system. *J Biol Chem* 276:48309–48317.
23. Oka T, *et al*. (2006) Cardiac-specific deletion of Gata4 reveals its requirement for hypertrophy, compensation, and myocyte viability. *Circ Res* 98:837–845.
24. Bisping E, *et al*. (2006) Gata4 is required for maintenance of postnatal cardiac function and protection from pressure overload-induced heart failure. *Proc Natl Acad Sci USA* 103:14471–14476.
25. Nagueh SF, *et al*. (1997) Doppler tissue imaging: A noninvasive technique for evaluation of left ventricular relaxation and estimation of filling pressures. *J Am Coll Cardiol* 30:1527–1533.
26. Zile MR, Brutsaert DL (2002) New concepts in diastolic dysfunction and diastolic heart failure. Part II: Causal mechanisms and treatment. *Circulation* 105:1503–1508.
27. Warnes CA (2005) The adult with congenital heart disease: Born to be bad? *J Am Coll Cardiol* 46:1–8.
28. Webb G, Gatzoulis MA (2006) Atrial septal defects in the adult: Recent progress and overview. *Circulation* 114:1645–1653.
29. Norozi K, *et al*. (2006) Incidence and risk distribution of heart failure in adolescents and adults with congenital heart disease after cardiac surgery. *Am J Cardiol* 97:1238–1243.
30. Meyer-Wittkopf M, Cooper S, Vaughan J, Sholler G (2001) Three-dimensional (3D) echocardiographic analysis of congenital heart disease in the fetus: Comparison with cross-sectional (2D) fetal echocardiography. *Ultrasound Obstet Gynecol* 17:485–492.
31. Pawelec-Wojtalik M, Wojtalik M, Mrowczynski W, Surmacz R, Quereshi SA (2006) Comparison of cardiac function in children after surgical and Amplatzer occluder closure of secundum atrial septal defects. *Eur J Cardiothorac Surg* 29:89–92.
32. De Backer JF, et al. (2006) Primary impairment of left ventricular function in Marfan syndrome. *Int J Cardiol* 112:353–358.
33. Luo W, *et al.* (1994) Targeted ablation of the phospholamban gene is associated with markedly enhanced myocardial contractility and loss of beta-agonist stimulation. *Circ Res* 75:401–409.
34. Gramolini AO, *et al*. (2006) Cardiac-specific overexpression of sarcolipin in phospholamban null mice impairs myocyte function that is restored by phosphorylation. *Proc Natl Acad Sci USA* 103:2446–2451.
35. Asahi M, *et al*. (2004) Cardiac-specific overexpression of sarcolipin inhibits sarco(endo)plasmic reticulum Ca^{2+} ATPase (SERCA2a) activity and impairs cardiac function in mice. *Proc Natl Acad Sci USA* 101:9199–9204.
36. Gramolini AO, *et al*. (2004) Sarcolipin retention in the endoplasmic reticulum depends on its C-terminal RSYQY sequence and its interaction with sarco(endo)plasmic Ca(2+)-ATPases. *Proc Natl Acad Sci USA* 101:16807–16812.
37. McDermott DA, *et al.* (2005) TBX5 genetic testing validates strict clinical criteria for Holt-Oram syndrome. *Pediatr Res* 58:981–986.